# Planning Collision-Free Trajectories for Reversing Multiply-Articulated Vehicles

Amy J. Rimmer, David Cebon

***Abstract* – a global path-planning strategy is proposed which defines the geometric path of the rear trailer axle of a multiply-articulated vehicle travelling in reverse. This is intended for use in conjunction with a path-tracking reversing controller. A general, multiple-trailer vehicle model is derived and used to model a 'B-double' heavy vehicle combination, which has two trailers. The curvature properties of a path for the rear trailer axle are investigated and an empirical relationship is defined between the curvature and the length over which the curvature changes. This is used to generate a library of feasible path segments and the vehicle model is used to calculate swept paths. A Dijkstra grid search algorithm is then used to connect the path segments together to generate a collision-free composite path. An example path generation is presented for the B-double.**

***Index Terms*— articulated vehicle, path planning, reversing**

## I. Introduction

Multiply-articulated vehicles can be found in the road-freight industry throughout the world. Using longer heavy vehicles can give a reduction (up to 30%) in fuel consumption when compared with conventional heavy vehicles. Benefits also include reduced road wear (40%) and fewer heavy vehicles on the roads (44%) [1, 2].

Reversing multiply-articulated heavy vehicles tends to be avoided where possible because they can only be reversed by highly skilled drivers [3]. A semi-autonomous system for reversing these vehicles would prove useful in the efforts to introduce longer vehicles more widely. In order to implement such a system, an algorithm for planning collision-free trajectories for multiply-articulated vehicles is needed, as is a system for path-tracking control (see [4]).

Planning collision-free trajectories for articulated vehicles has been investigated in the literature. Path planning (also known as 'motion planning') is a vast area of research and the articulated vehicle presents a particularly challenging problem due to its nonholonomic property and the fact that it is unstable in reverse.

Methods have been published for vehicles with single-trailers and multiple-trailers. The hitch points (location where one vehicle couples to another) are most commonly assumed to be located at the longitudinal position of the axles of the vehicle units ahead (known as 'on-axle' hitching), though they can also be assumed to be located in front or behind the axles ahead (known as 'off-axle' hitching).

The 'two step' method involves the use of a holonomic planner followed by a path conversion to ensure it complies with the nonholonomic constraints. This has been implemented in practice on a two-wheeled robot (with differential drive) pulling a trailer [5]. A similar approach to the two step method assumes a 'semi-holonomic' system (instead of a holonomic one) which is obtained by removing some, but not all, of the nonholonomic constraints on the vehicle [6]. This produces smoother paths with fewer cusps. A drawback of the two step approach is that the conversion from the holonomic to the nonholonomic path may result in an undesirable solution: it may be long and have many cusps.

Stahn et al [7] implemented a grid search on a full-scale rigid truck with a trailer. A 'Rapidly exploring Random Tree' (RRT) was used for a 3-trailer vehicle [8] with on-axle hitching but the performance was not repeatable as some runs failed to calculate a feasible path. Additional examples include using feasible velocity polygons [9], a least squares approach [10], and model predictive control [11].

In summary, the examples of path planning for reversing of multiply-articulated vehicles found in the literature all have limitations, such as algorithm runtime and repeatability. Some assume on-axle hitching [5, 6, 8, 11], or that hitching is behind the axle [9, 10]. A few have only been demonstrated for vehicles with one trailer [5, 7, 11]. A summary of approaches found in the literature for path planning for articulated vehicles is shown in Table 2. Many papers investigated do not state the algorithm runtime.

This paper will present an alternative approach to path planning for multiply-articulated vehicles. The main focus will be ensuring the path satisfies the vehicle steer limits and steer rate limits. This includes an investigation into the curvature requirements of a path for a multiply-articulated vehicle. The path building process is then presented and a case study example is shown.

The approach proposed for global path planning is as follows. The initial inputs are the start and end points of the path. Obstacles are defined and the vehicle limits are converted into constraints on the path curvature. A geometric path is then constructed from the start

This paper was submitted for review on XXth February 2015. This research was funded by the Engineering and Physical Sciences Research Council (EPSRC) and Volvo Trucks through an Industrial CASE award.

A. J. Rimmer and D. Cebon*, Department of Engineering, University of Camrbridge, Trumpington Street, Cambridge, CB2 3AP, UK

*Corresponding author dc@eng.cam.ac.uk

configuration to the end configuration using pre-computed track segments. The path is then checked for collisions through a vehicle simulation and the path is modified if needed. The strategy described in this paper differs from the approaches used in the literature because it focuses on planning the geometry of the path rather than creating a set of model inputs (known as 'motion planning').

## II. Vehicle Model

A model of a multiply-articulated vehicle was implemented in MATLAB®. In order to fit with the global path-planning strategy, a vehicle model that could predict the vehicle positions based on the geometric path of the rear trailer was devised. This was achieved using a kinematic approach, which assumed that each axle group can be represented by a single wheel with zero sideslip.

Kinematic vehicle models are often used for path planning of articulated vehicles [5-11]. These usually have two inputs: the longitudinal speed of the tractor unit and the steer angle of the front axle. The kinematic model presented here differs slightly from the normal approach, as it works backwards form the rearmost vehicle unit, controlling the angular velocity of the unit and keeping the longitudinal speed constant. This enables the vehicle states and positions to be calculated for a given path of the rear trailer. For a kinematic model, motion is the same in the forwards and reverse directions for a given path.

The following assumptions were made when deriving the model:

1 The effects of vehicle roll and pitch were neglected (yaw only model)
2 The effect of lateral load transfer was neglected
3 The front axle of the first unit had perfect Ackerman geometry
4 No sensor noise or other sensor imperfections
5 No saturation or rate limits
6 Inertial forces were neglected
7 Each axle group can be modelled by a single rolling wheel, whose lateral velocity is always zero

These assumptions were possible because reversing and manoeuvring are carried out at low speeds so inertial forces and the effects of lateral load transfer, pitch and roll are negligible. HGVs generally have excellent steering geometry to reduce tyre wear. For the purpose of this paper, it is assumed that accurate information on vehicle states is available and that the steering won't saturate although it is intended to only operate within the steering limits. Winkler [12] showed that an axle group can be modelled by a single rolling wheel. These assumptions and modelling approach are in line with others in the path-planning literature [5-11, 15].

The model was derived for a vehicle with an arbitrary number of trailers ($n$). By appropriate choice of parameters, this general model can be used to model the low-speed behaviour of essentially any multiply-articulated vehicle. A model diagram is shown in Figure 1 for the two-trailer case ($n$ = 2).

For a tractor unit with $n$ trailers, this will result in a vehicle with $n$+1 units and $n$ articulation joints. Index '$i$' will be used to denote the unit number, where $i$ = 1 is used for the tractor unit, $i$ = 2 for the first trailer etc.

### A. Derivation

Detailed diagrams of a tractor unit and a general trailer unit for the kinematic model are shown in Figure 2. These show the geometries and velocities used in the derivation.

The state vector, **z**, contains all the articulation angles:

$$\mathbf{z} = \begin{bmatrix} \Gamma_1 \\ \vdots \\ \Gamma_n \end{bmatrix}, \dot{\mathbf{z}} = \begin{bmatrix} \dot{\Gamma}_1 \\ \vdots \\ \dot{\Gamma}_n \end{bmatrix} \tag{1}$$

where $\Gamma_j$ represents the articulation angle between the $j$th and ($j$+1)th vehicle unit.

The model input is the path of the axle on the rearmost trailer ($x_{n+1}$, $y_{n+1}$). This must have continuous curvature and start and end with straight segments. The path heading ($\theta_{n+1}$) and distance travelled ($s_{n+1}$) are calculated from the position of the rearmost trailer:

$$\theta_{n+1} = \tan^{-1}\left(\frac{dy_{n+1}}{dx_{n+1}}\right) \tag{2}$$

$$s_{n+1_p} = \sum_{m=1}^{p} \sqrt{\left(\Delta y_{n+1_m}\right)^2 + \left(\Delta x_{n+1_m}\right)^2} \tag{3}$$

where $m$ denotes the time step and $p$ is the current time step.

The angular velocity, $\Omega_{n+1}$, is then calculated:

$$\Omega_{n+1} = \frac{d\theta_{n+1}}{ds_{n+1}} u_{n+1} \tag{4}$$

where $u_{n+1}$ is the longitudinal velocity of the last vehicle unit.

For a given vehicle unit $i$, the (zero) lateral velocity at the wheel of the $i$-1th vehicle unit can be calculated:

$$v_{i-1} = \left(v_i + l_i\Omega_i\right)cos\left(\Gamma_{i-1}\right) + u_i sin\left(\Gamma_{i-1}\right) + \left(\Omega_i - \dot{\Gamma}_{i-1}\right)c_{i-1} = 0 \tag{5}$$

Here $u_i$ , $v_i$ and $\Omega_i$ are the longitudinal, lateral and rotational velocities at the axle of the $i$th vehicle unit, $l_i$ and $c_i$ are the wheelbase and hitch offsets of the $i$th vehicle unit respectively, as shown in Figure 2.

Equation (5) can be rearranged to form an Ordinary Differential Equation (ODE):

$$\dot{\Gamma}_{i-1} = f_k\left(\Gamma_{i-1}, u_i, \Omega_i, l_i, c_{i-1}\right) \tag{6}$$

Equation (6) can be solved for $\Gamma_{i-1}$ using an ODE solver. The longitudinal and angular velocity of the axle on the $i$-1th unit can then be calculated:

$$\Omega_{i-1} = \Omega_i - \dot{\Gamma}_{i-1} \tag{7}$$

$$u_{i-1} = u_i cos\left(\Gamma_{i-1}\right) - \left(v_i + l_i\Omega_i\right)sin\left(\Gamma_{i-1}\right) \tag{8}$$

Some observer states were added to measure the heading and position of each vehicle unit:

$$\dot{\theta}_i = \Omega_i \tag{9}$$

$$\dot{x}_i = u_i cos(\theta_i) - v_i sin(\theta_i) \tag{10}$$

$$\dot{y}_i = u_i sin(\theta_i) + v_i cos(\theta_i) \tag{11}$$

where $x_i, y_i$ and $\theta_i$ are the position and heading of the axle of the vehicle unit (the rear axle in the case of the first unit).

The ODE solver will only work if the pair of vehicle units (or joint) is simulated in the stable direction. Figure 3 shows the stable directions for joints if the motion is driven by the axle on the rear vehicle unit. If the hitch offset is positive ($c_{i-1} > 0$), the vehicle is simulated in the reverse direction ($u_i < 0$). If the hitch offset is negative ($c_{i-1} < 0$), the vehicle is simulated in the forwards direction ($u_i > 0$).

The articulation angles, and velocities and positions of each vehicle unit can be calculated for a given path of the rear trailer axle using Equations (3) to (11) and propagating up the vehicle, starting with the rearmost vehicle unit. The front axle steer angle can then be defined:

$$\delta = \tan^{-1} \frac{(\Omega_1 l_1)}{u_1} \tag{12}$$

### B. The B-double

The main vehicle combination investigated in this paper is the ‘B-double’. The B-double has a tractor unit, a B-trailer and a semitrailer. A B-trailer is a special trailer which has an additional fifth wheel coupling that enables connection of another semitrailer. Vehicle parameters for a B-double vehicle are shown in Table 1. These were based on the geometry of a full-size B-double test vehicle [4]. Winkler’s approach was used to determine the position of the equivalent wheel for trailers with multiple axles [12].

## III. Path Curvature Requirements

It was necessary to define some geometric constraints on the path curvature to comply with the nonholonomic property and steer limits of the vehicle. The literature indicates that continuous curvature is required for a nonholonomic vehicle, such as a car [13]. Continuous curvature is commonly achieved with clothoids, which are paths of linearly varying curvature [13]. In [14], an articulated vehicle with on-axle hitching is investigated and it is suggested that the path of the trailer must be $G^4$ (continuous in the fourth derivative of the path) to be feasible. It is however not known what constraints are needed when defining the path of a trailer axle for a multiply-articulated vehicle with off-axle hitching.

### A. Vehicle Limits

In previous research using a B-double test vehicle, the maximum steer angle limit of the tractor unit was 45° and the maximum steer rate of the steering actuator hardware was 18°/s [4]. A limit of 9°/m was chosen for the change in steer angle with distance. This limit assumes the vehicle is travelling at -1m/s and is half the physical limit to account for practical implementation issues such as sensor noise and actuator delays.

### B. Case Study on the B-double

Paths (of the rear trailer axle) with specified curvature properties were defined and tested to see if the B-double could manoeuvre the path within the steer limits. Three different paths were generated with continuous curvature and continuous first and second derivatives of curvature respectively. For each path, the curvature started at zero, increased to 0.1m$^{-1}$ (corresponding to a 10m radius) and then decreased back to zero. All three paths changed curvature over the same length (20m).

The vehicle model described in Section 2 was used to calculate the required front axle steer angles for the B-double in order for the rear trailer axle to follow the three different paths in reverse. This was done for two cases: assuming on-axle hitching (c = 0) and using the hitch offsets defined in Table 1. The resulting steer angles and steer rates are shown in Figure 4 with hitching both on-axle and off-axle for all three paths.

The steer angles and steer rates show sharp peaks for the first path (continuous curvature, Figure 4(a, b)), particularly for the off-axle hitching case. The steer angles and steer rates are smoother for the second path (continuous curvature derivative, Figure 4(c, d)), but there are still some peaks in the steer rate for the vehicle with off-axle hitching. The third path (continuous curvature second derivative, Figure 4(e, f)) shows the smoothest results with no sharp peaks for either case, and also keeps within the 9°/m steer rate limit.

The results from the B-double case study indicate that the path of the n$^{th}$ trailer must have continuous curvature to the n$^{th}$ derivative. This relationship was suggested in [4] for any number of trailers from open loop simulations of a kinematic vehicle model with multiple trailers and on-axle hitching. This conclusion disagrees with the relationship suggested in [14].

The method for constructing the third path, with continuous curvature second derivative, was used in this research to make paths for the B-double combination. Using this approach, it was much easier to comply with the steer rate limits of 9°/m.

### C. Relationship between Transient Length and Curvature

From simulations with the vehicle model described in Section 2, no direct relationship could be formed between steer rate limit and path curvature derivative. Therefore, in order to construct paths, an empirical relationship was calculated for the B-double to ensure that the path complied with the vehicle rate limits. A ‘transient length’ was defined as the path length over which the curvature changes from zero to a desired value, as illustrated in Figure 5(a).

‘Transient lengths’ were calculated for a range of curvatures, which were checked to ensure the steer rate did not exceed 9°/m. The relationship between curvature and ‘transient length’ is shown in Figure 5(b). The resulting heading change was also calculated by integrating the curvature with respect to the distance along the path, shown in Figure 5(c). These empirical values were used in a lookup table to construct feasible paths for the B-double vehicle combination.

## IV. Path Definition

The path definition method was analogous to the process of building model car tracks using a set of track segments. It was therefore named the 'car track' method. An outline of the path definition process is shown in Figure 6. An offline calculation was performed for each vehicle type, which used the relationship between transient length and curvature to generate a library of feasible path segments. These segments were then used to construct a 3D grid and a grid search was conducted for each path-planning task. The grid search included obstacle avoidance.

### A. Feasible Path Segments

The set of feasible path segments was defined to comply with the steer angle limit and steer rate limit, using the empirical relationships derived in Section 3.3. These path segments were straight lines, lane changes and turns of various geometries (examples shown in Figure 7). The paths were defined such that they started and ended on a 5m 2D grid. All headings started and ended at multiples of 45 degrees and all curvatures were zero at the beginning and end of the path segments so they could be joined together to create a composite path.

The swept path of the vehicle for each path segment was calculated using the vehicle model outlined in Section 2, with the vehicle parameters from Table 1. This calculation was done assuming that the end of each manoeuvre was a long straight, giving time for the vehicle to settle into straight start and end configurations. The swept paths are plotted in Figure 7 for all eight path segments.

In most cases, the swept path extends beyond the start point of the path because the vehicle needs space to prepare to negotiate the path. When the path segments were joined together to make a composite path, the extended swept paths were included to ensure that the combined path did not hit any obstacles.

### B. Grid Search

A 'state lattice' approach has been used for various path planning applications in [15-18]. This approach defines an N-dimensional lattice where each point on the lattice corresponds to a model state. The states are joined together by 'motion primitives', which are feasible paths for the given model. The path is then calculated by searching the state lattice for an optimal sequence of states.

The state lattice approach was used in this application to calculate a set of feasible path segments to get from a desired start configuration to a goal configuration. A 3D grid was used; the three dimensions were position (x and y) and heading (θ). The grid resolution was 5m in the x and y directions and the heading was discretised at 45°. The feasible path segments were defined such that they started and ended at grid points. A set of additional manoeuvres was required for the diagonal cases (not shown in Figure 7). The grid was created by defining a 3D matrix for a certain area, with 8 different horizontal planes representing the possible headings (0°, 45°, 90°, 135°, 180°, 225°, 270°, and 315°).

At each point on the grid, there are 15 feasible paths to the next grid point. For a given heading, there are 8 manoeuvres in total, 7 of which can be mirrored. An illustration of the paths and positions of the resulting 'nodes' is shown in Figure 8 for a grid point starting at the origin with zero heading. A pre-defined 'cost' was calculated for each 'node', which was a combination of the length of the manoeuvre and the heading change.

$$J = w_h \left|\theta_{p2} - \theta_{p1}\right| + w_l s_p \tag{13}$$

where $w_h$ and $w_l$ are the weightings for heading and length respectively, $\theta_{p1}$ and $\theta_{p2}$ are the headings at the start and end of the path respectively and $s_p$ is the length of the path.

The Dijkstra grid search algorithm [19] was adopted to carry out the grid search. The process is briefly summarised in the Appendix. Proposed path segments were checked for collisions with obstacles during the grid search calculation, which meant that the grid could be calculated offline and used in any environment with obstacles.

Once the grid points were defined, the path was constructed by joining the path segments together. Because the swept paths have been checked, this approach almost guarantees collision avoidance. It is not completely guaranteed, however, because the resultant swept path from joining two path segments together may differ slightly from the individual swept paths of each path segment.

### C. Collision Avoidance

To investigate the differences in swept path, a study was performed for all possible combinations of path segment pairs. For each pair, the swept path was calculated using the vehicle simulation and then compared with the swept path predicted from combining the swept paths of the individual segments. An error was recorded if the overall swept path exceeded the swept paths of the individual segments. A total of 450 different combinations were investigated (2 sets of 8 different paths, 7 of which can change direction).

A histogram showing the resulting errors is shown in Figure 9. The swept path differences ranged from 0 to 0.58m with a mean of 0.26m. Collision avoidance would be guaranteed if an additional clearance (safety margin) of 0.58m was used for obstacles. An alternative solution could be to precompute the swept paths of all combinations of segments and use this swept path in the algorithm. With either approach, the 'path modification' step in the global path planning strategy is not needed, which significantly simplifies the procedure.

## V. Case Study

In order to test the path planning method presented here, a path planning task was set up. This had a 200m by 200m 2D plane with some arbitrary obstacles and specified start and goal positions, as shown in Figure 10. The grid search was conducted for this task and the resulting path is shown in Figure 10, which also shows the obstacles and the chosen grid points. The resulting path is feasible and indicates the algorithm was run successfully. The grid search took 20 seconds to run in uncompiled MATLAB® code on a conventional PC.

Figure 11 shows the resulting vehicle swept example for the path shown in Figure 10. The swept path predicted by the feasible path segments is shown along with the actual swept path calculated using the vehicle model. Due to the extended sections of swept path, some of the segments overlap. If the outermost swept path is compared with the overall swept path, there is no noticeable difference. The interference calculation was carried out for the case study path and no collisions were detected.

Table 2 presents a comparison between the method proposed in this paper and other methods found in the literature. The algorithm runtime is faster (considering the path distance) than any of the algorithm runtimes listed. However, many of the examples found in the literature produce paths with cusps whilst the algorithm presented in this paper does not include cusps.

## VI. Conclusions

(i) A ‘car track’ strategy was proposed for global path planning using the geometry of the path instead of the conventional approach of generating a set of model inputs. This strategy could be used in conjunction with a path-following reversing controller.

(ii) For a vehicle with n trailers, the path of the rear trailer must have continuous curvature to the n$^{th}$ derivative for the required front axle steer rate to be smooth.

(iii) A set of feasible path segments was generated and the corresponding swept path was calculated for the B-double travelling in reverse.

(iv) A version of the Dijkstra grid search algorithm was used to join feasible paths together to get from the start configuration to the goal configuration, while minimising the value of a cost function. This algorithm checked the swept path and almost guaranteed collision avoidance.

(v) An analysis of all possible combinations of path segment pairs showed the maximum discrepancy between predicted and actual swept paths was 0.58m. Collision avoidance could be guaranteed using by adding this safety margin for obstacle positions.

(vi) The swept path calculated using the feasible path segments agrees well with the swept path calculated by simulating the vehicle motion over the entire path.

(vii) A case study successfully demonstrated the approach and generated an interference-free path.

Future work will involve reducing the resolution of the grid and speeding up the calculation. Additionally, ‘cusps’ (changes in direction) could be introduced to the algorithm.

## VII. Nomenclature

| | |
|---|---|
| $c$ | Distance from rear axle of tractor unit or first axle of trailer to rear hitch point [m] |
| $f_k$ | Ordinary differential equation function for kinematic vehicle model |
| $fo$ | Distance from front axle or front hitch point to front of vehicle unit[m] |
| $l$ | Wheelbase of vehicle unit [m] |
| $n$ | Number of trailers |
| $ro$ | Distance from rear axle of tractor unit or first axle of trailer to rear of vehicle unit[m] |
| $s$ | Distance travelled [m] |
| $u$ | Longitudinal velocity of vehicle unit [m/s] |
| $v$ | Lateral velocity of vehicle unit at the rear axle for the kinematic model or at the CoG for the dynamic model [m/s] |
| $wd$ | Width of vehicle unit [m] |
| $w_h$ | Cost function weighting on heading change |
| $w_l$ | Cost function weighting on path length |
| $x$ | Longitudinal position of vehicle unit [m] |
| $y$ | Lateral position of vehicle unit [m] |
| $\mathbf{z}$ | State vector of vehicle model |
| $\boldsymbol{J}$ | Cost function for grid search algorithm |
| $\delta$ | Tractor unit front axle steer angle [rad] |
| $\theta$ | Heading angle of vehicle unit [rad] |
| $\kappa$ | Curvature of path [m$^{-1}$] |
| $\Gamma$ | Articulation angle [rad] |
| $\Omega$ | Yaw angular velocity [rad/s] |
| $\dot{\ }$ | First derivative with respect to time |
| $\ddot{\ }$ | Second derivative with respect to time |
| $_i$ | Corresponding to i$^{th}$ vehicle unit |
| $_j$ | Corresponding to articulation joint between j$^{th}$ and j+1$^{th}$ vehicle unit |
| $_n$ | Corresponding to the last articulation joint |

## Appendix: Implementation of Dijkstra Grid Search [19]

(i) An ‘open set’ is defined as all possible grid points.

(ii) A ‘cost’ is defined for each grid point. This is initially set to infinity for all points except the start configuration, which is set to zero.

(iii) An iterative loop searches the grid:

a. A ‘current vertex’ is defined as the grid point in the ‘open set’ with the lowest ‘cost’.

b. The ‘adjacent’ grid points are identified (i.e. those that can be joined by paths as shown in Figure 8) and their ‘costs’ are calculated as the current ‘cost’ plus the ‘cost’ of the ‘node’ which joins them to the ‘current vertex’.

c. For each adjacent grid point, if the calculated ‘cost’ is lower than the existing ‘cost’, the ‘cost’ information is updated. In this case, the ‘current vertex’ is logged to record the ‘parent’ of the corresponding ‘cost’ information.

d. Once all adjacent grid points have been processed, the ‘current vertex’ is removed from the ‘open set’

(iv) The algorithm stops when the ‘current vertex’ is the goal configuration.

(v) The optimum set of grid points is identified using the ‘parent’ information logged during the ‘cost’ update phase in (iii, c).

## VIII. Acknowledgements

The authors would like to acknowledge the members of the Cambridge Vehicle Dynamics Consortium (CVDC) who supported the work in this project. At the time of writing, the Consortium consists of the University of Cambridge with the following partners from the heavy vehicle industry: Anthony Best Dynamics, Camcon, Denby Transport, Firestone Air Springs, GOODYEAR DUNLOP, Haldex, Mektronika Systems Ltd, Motor Industry Research Association, SDC Trailers, SIMPACK, Tinsley Bridge, Tridec, Volvo Trucks, and Wincanton.

The authors would like to acknowledge Leo Laine and Carl-Johan Hoel of Volvo Trucks for their collaboration and support throughout the project. The authors would also like to acknowledge Tim Hennock of the University of Cambridge for his technical contributions to the research during a mathematics summer project.

## IX. References

1. Odhams AMC, Roebuck RL, Lee YJ, Hunt SW, and Cebon D. Factors influencing the energy consumption of road freight transport. *Proceedings of the Institution of Mechanical Engineers, Part C: Journal of Mechanical Engineering Science*, 2010; 224(9): 1995-2010
2. Woodrooffe J and Ash L, *Economic Efficiency of Long Combination Transport Vehicles in Alberta*, Prepared for Alberta Infrastructure, Woodrooffe and Associates, Canada. 2001
3. Kjell M and Westerlund KR, Feasibility of Longer Combination Vehicles. Chalmers University of Technology, *Dissertation submitted for the degree of Masters*, 2009
4. Rimmer AJ, Autonomous Reversing of Multiply-Articulated Heavy Vehicles. University of Cambridge, *Dissertation submitted for the degree of Doctor of Philosophy*, 2014
5. Sekhavat S, Lamiraux F, Laumond JP, Bauzil G, and Ferrand A. Motion planning and control for Hilare pulling a trailer: experimental issues, *Proceedings of the IEEE International Conference on Robotics and Automation (IRCA)*, Albuquerque, New Mexico, 1997
6. Sekhavat S, Svestka P, Laumond J-P, and Overmars MH. Multilevel Path Planning for Nonholonomic Robots Using Semiholonomic Subsystems. *The International Journal of Robotics Research*, 1998; 17(8): 840-857
7. Stahn R, Stark T and Stopp A. Laser scanner-based navigation and motion planning for truck-trailer combinations, *Proceedings of the IEEE/ASME International Conference on Advanced Intelligent Mechatronics*, Zürich, Switzerland, 2007
8. Cheng P, Shen Z and LaValle SM. RRT-Based Trajectory Design for Autonomous Automobiles and Spacecraft. *Archives of Control Sciences*, 2001; 11(3-4): 167-194
9. Quintero-Alvarez P, Ramirez G and Zeghloul S. A collision-free path-planning method for an articulated mobile robot. *Applied Bionics and Biomechanics*, 2007; 4(2): 71-81
10. Divelbiss AW and Wen JT. A path space approach to nonholonomic motion planning in the presence of obstacles. *IEEE Transactions on Robotics and Automation*, 1997; 13(3): 443-451
11. Nayl T, Nikolakopoulos G and Gustafsson T. On-Line path planning for an articulated vehicle based on Model Predictive Control, *Proceedings of the Control Applications (CCA), 2013 IEEE International Conference on*, 2013
12. Winkler CB. Simplified Analysis of the Steady-State Turning of Complex Vehicles. *Vehicle System Dynamics*, 1998; 29(3): 141-180
13. Scheuer A and Fraichard T. Continuous-curvature path planning for car-like vehicles, *Proceedings of the IEEE/RSJ International Conference on Intelligent Robots and Systems (IROS)*, Grenoble, France, 1997
14. Ghilardelli F, Lini G and Piazzi A. Path Generation Using $\eta^4$-Splines for a Truck and Trailer Vehicle. *Automation Science and Engineering, IEEE Transactions on*, 2014; 11(1): 187-203
15. Pivtoraiko M, Knepper RA and Kelly A. Differentially constrained mobile robot motion planning in state lattices. *Journal of Field Robotics*, 2009; 26(3): 308-333
16. Pivtoraiko MN, Differentially Constrained Motion Planning with State Lattice Motion Primitives. Carnegie Mellon University, *Dissertation submitted for the degree of Doctor of Philosophy*, 2012
17. Pancanti S, Pallottino L, Salvadorini D, and Bicchi A. Motion planning through symbols and lattices, *Proceedings of the IEEE International Conference on Robotics and Automation (IRCA)*, New Orleans, 2004
18. Likhachev M and Ferguson D. Planning Long Dynamically Feasible Maneuvers for Autonomous Vehicles. *The International Journal of Robotics Research*, 2009; 28(8): 933-945
19. Minieka E, *Optimization algorithms for networks and graphs*, New York: Marcel Dekker, 1978

## X. Biographies

Amy Rimmer MEng, PhD, AMIMechE completed her PhD at the University of Cambridge in 2015. She collaborated with Volvo Trucks and other members of the Cambridge Vehicle Dynamics Consortium during her time at Cambridge. She is now a Research Engineer at Jaguar Land Rover, working on driverless car technologies.

David Cebon BE, PhD, FREng, FIMechE, is Professor of Mechanical Engineering. He is a Fellow of the Royal Academy of Engineering, Director of the Cambridge Vehicle Dynamics Consortium and the Centre for Sustainable Road Freight, as well as Managing Director of Granta Design Limited.  He is also a Fellow of Queens' College Cambridge.

Professor Cebon leads an active research group concerned with the design and dynamics of heavy vehicle suspensions, road damage and the micromechanics of asphalt failure. He also has interests in the use of computers in engineering design and education. He has written numerous papers on the dynamics of heavy vehicles, traffic instrumentation, road damage and materials information management software.

## XI. Tables

Table 1: Vehicle model parameters

| Parameter | | | Tractor | B-trailer | Semitrailer |
|---|---|---|---|---|---|
| Definition | Symbol | Unit | | | |
| Wheelbase | *l* | m | 3.7 | 8.89 | 7.85 |
| Axle to hitch | *c* | m | -0.16 | -0.35 | - |
| Front overhang | *fo* | m | 1.40 | 1.80 | 1.50 |
| Rear overhang | *ro* | m | 1.25 | 2.50 | 5.00 |
| Vehicle width (excluding mirrors) | *d* | m | 2.40 | 2.50 | 2.38 |

Table 2: Evaluation of planning methods

| Global path planner | | Vehicle Type | | Hitching | | Cusps? | | Optimisation | | | | Other | |
|---|---|---|---|---|---|---|---|---|---|---|---|---|---|
| | | Single trailer | Multiple trailers | On-axle | Off-axle | Yes | No | Feasibility | Number of cusps | Length | Distance from obstacles | Runtime [s] | Length of path [m] |
| Two step | [6] | | ▒ | ▒ | | ▒ | | | | ▒ | | ~60 | - |
| | [5] | ▒ | | ▒ | | ▒ | | ▒ | | | | 6 | 15 |
| RRT | [8] | | ▒ | ▒ | | ▒ | | ▒ | | | | - | - |
| grid search | [7] | ▒ | | | ▒ | ▒ | | ▒ | ▒ | ▒ | | 30 | 100 |
| Feasible velocities polygons | [9] | | ▒ | | ▒ | | ▒ | ▒ | | ▒ | | - | - |
| Least squares | [10] | ▒ | | | ▒ | ▒ | | ▒ | | | | 20 | 40 |
| MPC | [11] | ▒ | | ▒ | | | ▒ | | | ▒ | | - | - |
| Lattice | [15] | | ▒ | ▒ | | ▒ | | | | ▒ | | - | - |
| **'Car track' method** | | | ■ | | ■ | | ■ | ■ | | ■ | | 20 | 200 |

# XII. Figures

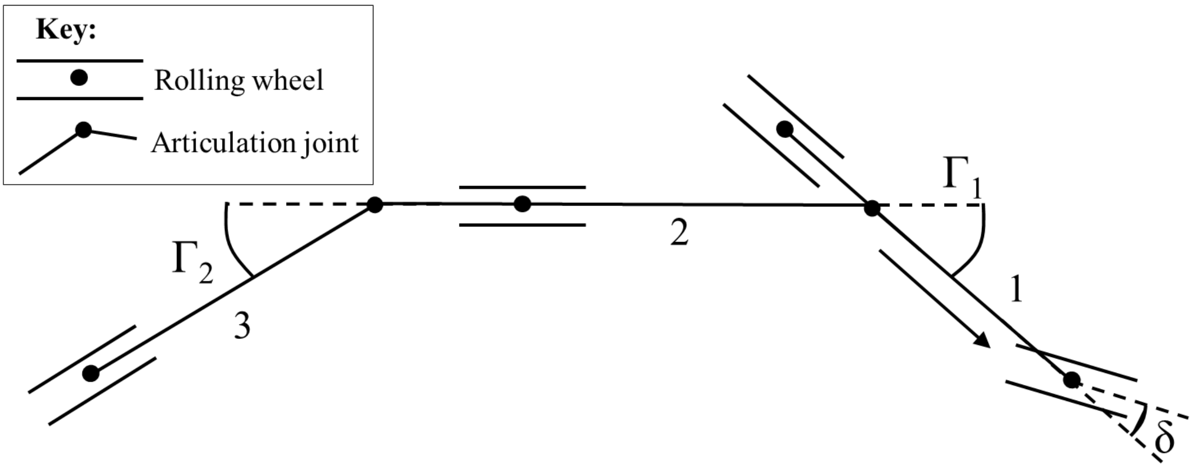

Figure 1: Kinematic vehicle model shown for the two-trailer case

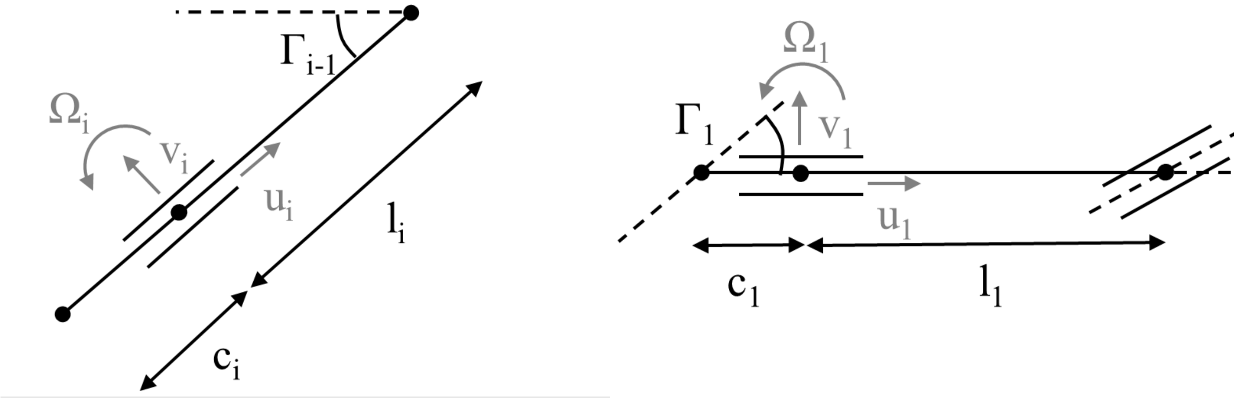

(a) (b)

Figure 2: Kinematic vehicle model showing (a) general trailer unit and (b) tractor unit.

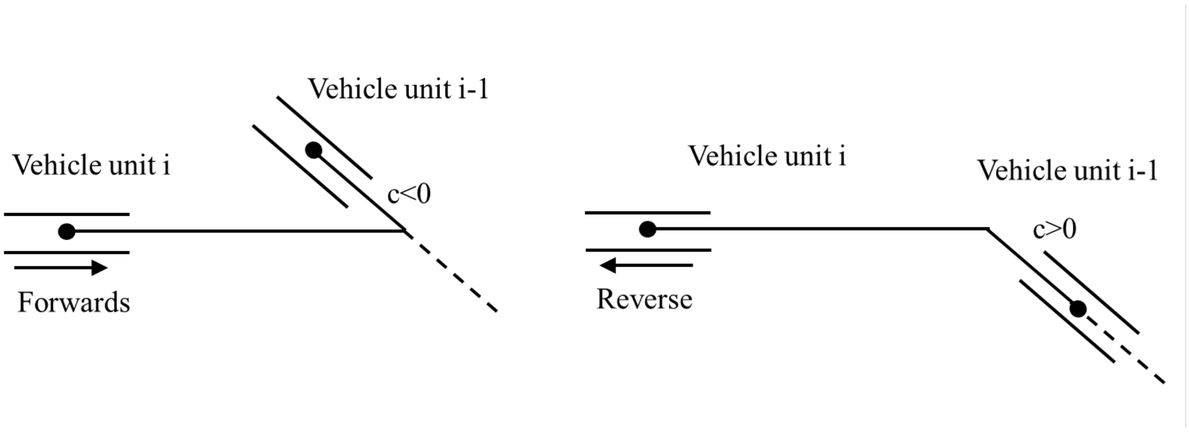

Figure 3: Diagram showing stable directions of motion for vehicles with negative and positive hitch offsets

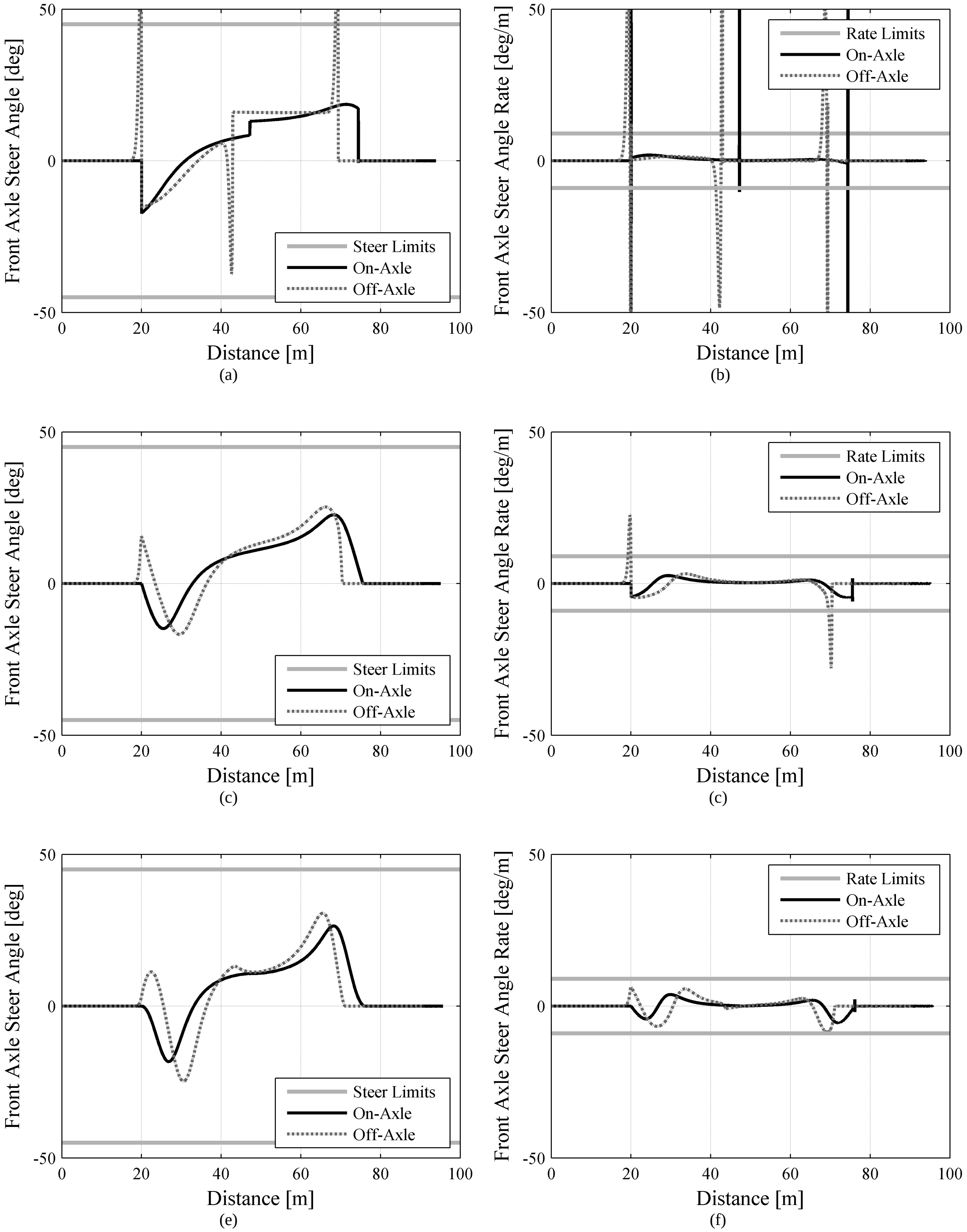

(a)

(b)

(c)

(c)

(e)

(f)

Figure 4: Resulting steer angles (a, c, e) and steer angle rates (b, d, f) when paths with continuous curvature (a, b), continuous curvature derivative (c, d) and continuous curvature second derivative (e, f) are tracked with a B-double vehicle using the vehicle model described in Section 2.

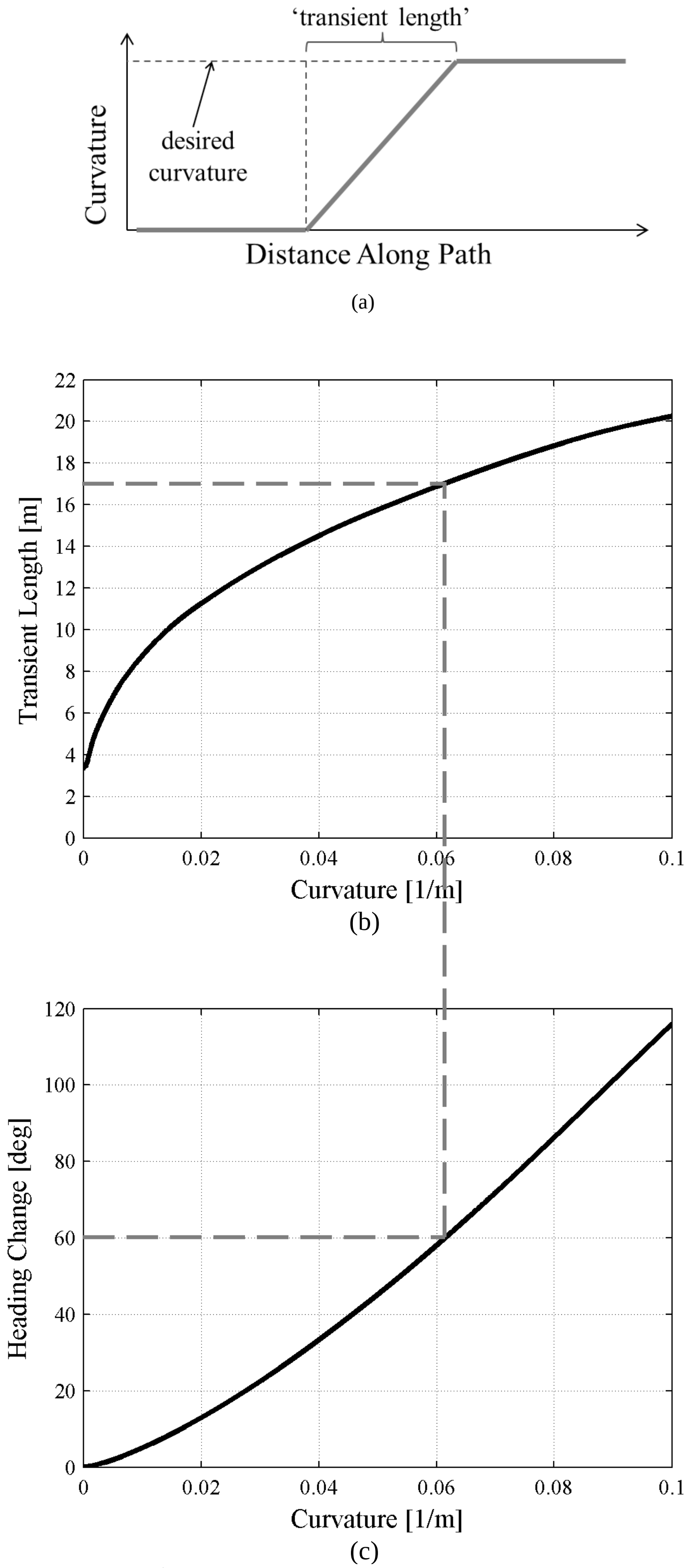

(a)

(b)

(c)

Figure 5: Illustration of 'transient length' definition (a). Empirical relationship between the desired curvature and the 'transient length' required to change from zero curvature to the desired curvature (b) and the resultant heading change (c) with curvature.

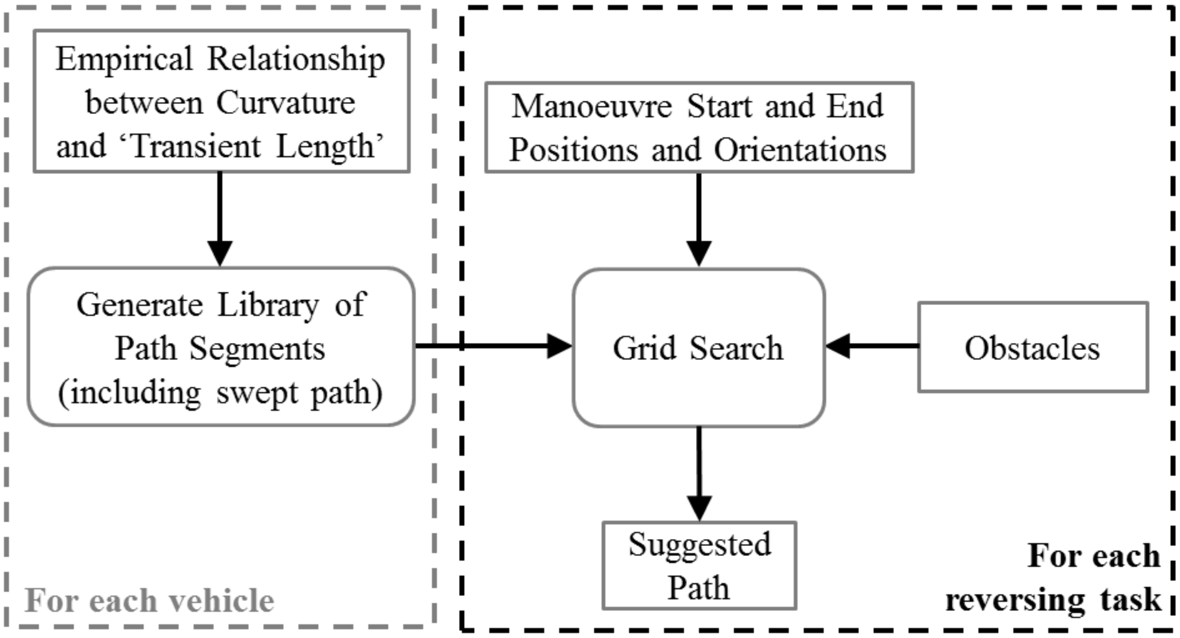
Empirical Relationship between Curvature and 'Transient Length'
Generate Library of Path Segments (including swept path)
For each vehicle
Manoeuvre Start and End Positions and Orientations
Grid Search
Obstacles
Suggested Path
For each reversing task

Figure 6: Flow chart for path definition phase, including grid search.

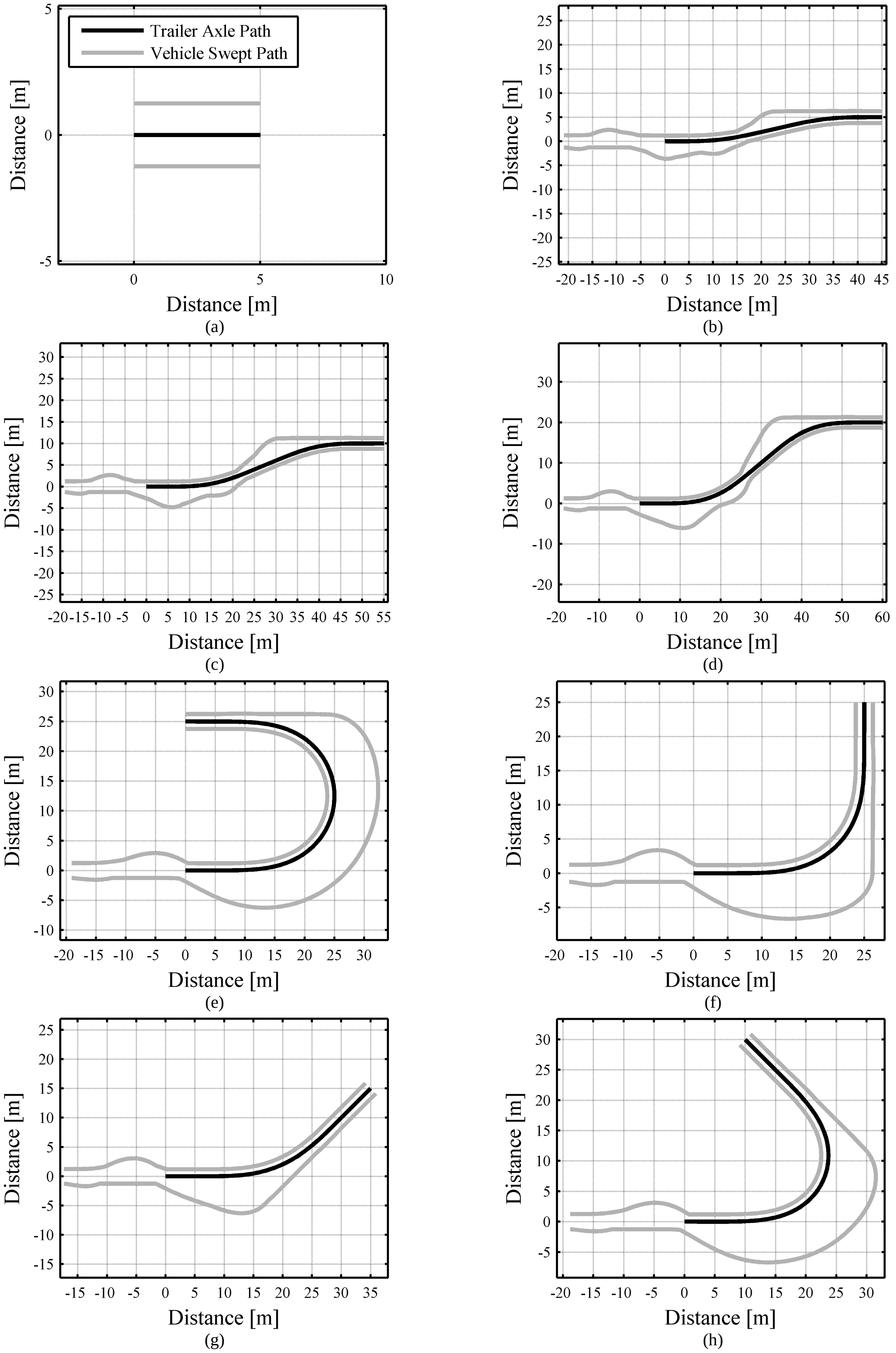

Figure 7: Feasible path segments and corresponding vehicle swept path for the B-double vehicle combination for headings at 0°, 90°, -90° and 180°. Paths include (a) straight line, (b)-(d) lane changes, (e) 180° turn, (f) 90° turn, (g) 45° turn, and (h) 135° turn

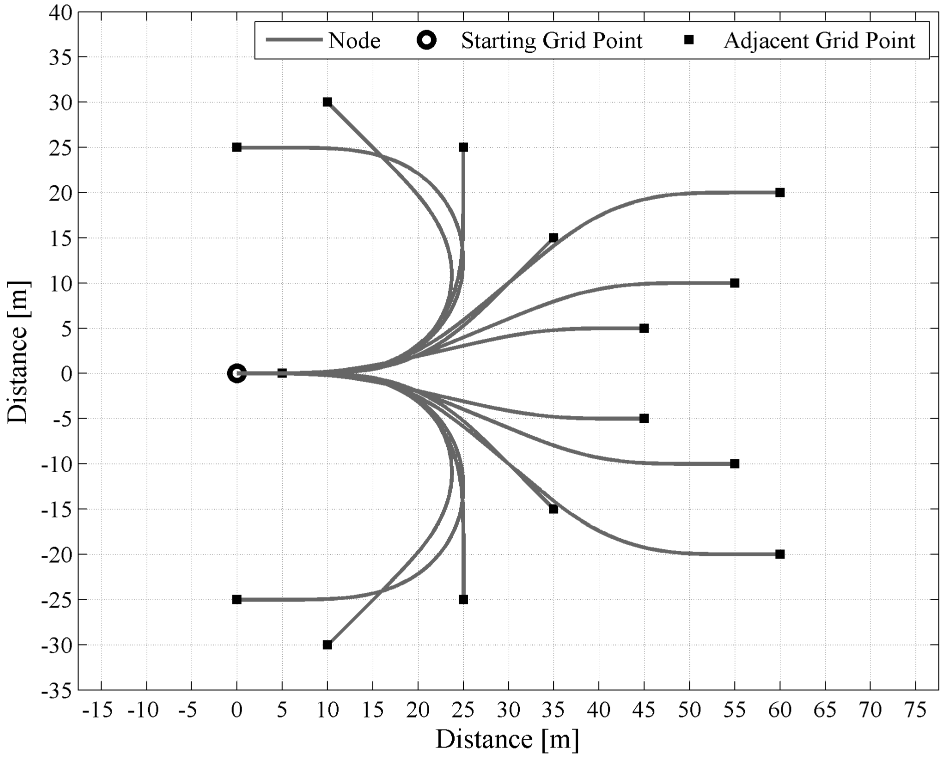

Figure 8: The 15 possible nodes created from the set of feasible path segments for a grid point starting at the origin with zero heading.

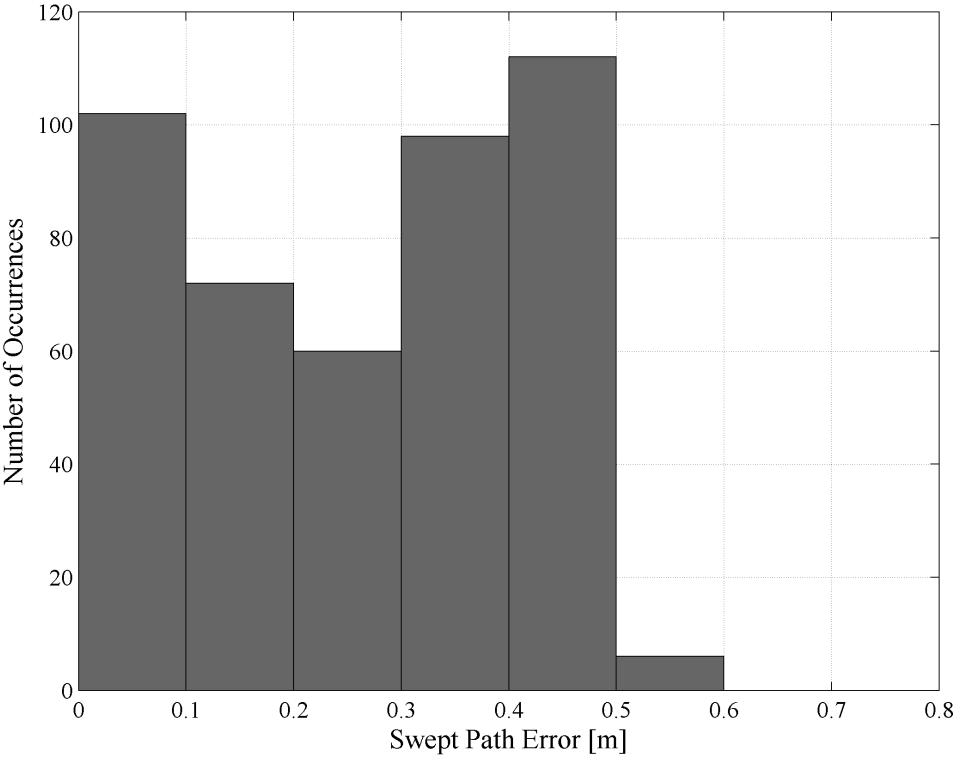

Figure 9: Histogram of vehicle swept path errors when comparing the actual swept path with those predicted using the path segments for all combinations of pairs of feasible paths.

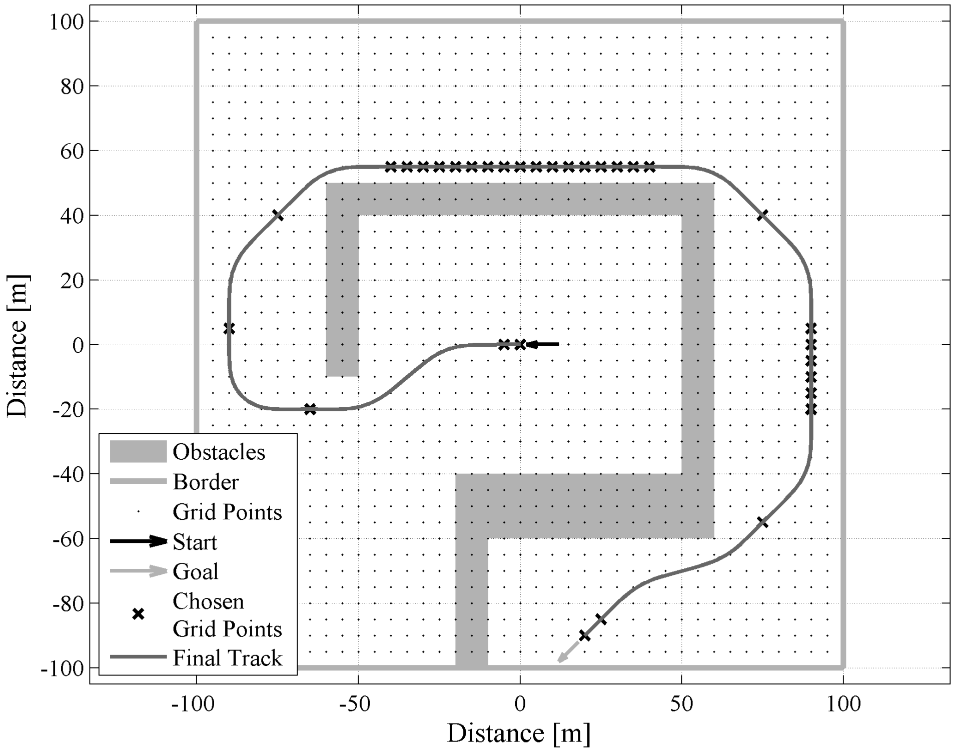

Figure 10: Path planning case study results including obstacles, grid points, selected grid points and the resultant path.

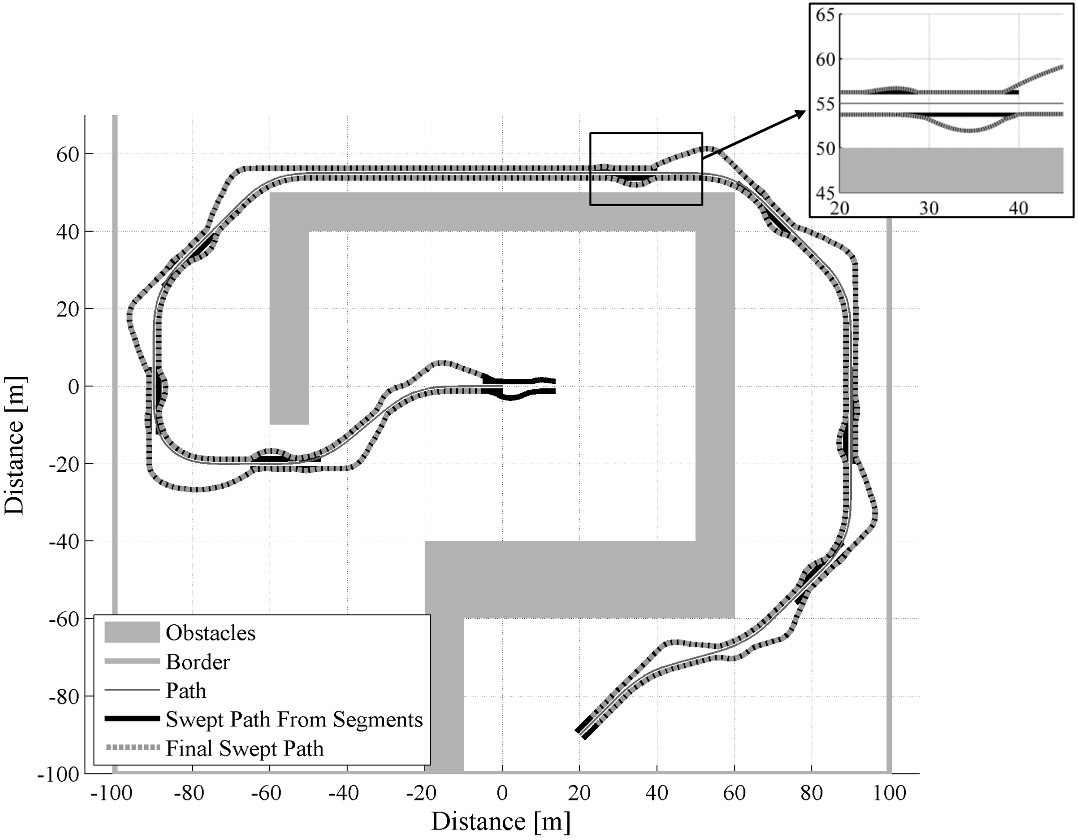

Figure 11: Resultant swept path of the B-double vehicle combination for the case study path. A comparison of the swept path predicted from the feasible path segments and the actual swept path from the vehicle model. A zoomed in section shows a join between two path segments.